

Miocene phosphorites from the Murray Ridge, northwestern Arabian Sea

Venigalla Purnachandra Rao^a, Ernst Hegner^b, Syed Wajih Ahmad Naqvi^a, Pratima Mohan Kessarkar^a, Syed Masood Ahmad^c, Datta Suryanarayana Raju^d

^a *National Institute of Oceanography, Dona Paula 403 004, Goa, India
(E-mail: vp rao@nio.org)*

^b *Department of Earth and Environmental Sciences, Ludwig-Maximilians-Universität, Luisenstraße 37, D-80333 München, Germany*

^c *National Geophysical Research Institute, Uppal Road, Hyderabad, India*

^d *Oil and Natural Gas Corporation, Dehradun, Uttarakhand, India*

Abstract

Phosphorites from the Murray Ridge, NW Arabian Sea comprise nodules, bioclasts, and bone fragments. The nodules are made up of a homogeneous, light-colored phosphate nucleus consisting of *Rivulariacean* filamentous cyanobacteria and a thin dark-grey colored phosphate cortex showing abundant microbial filaments and microborings. The bioclasts comprise ~14 - 14.5 Ma old planktonic foraminifers, accepted as the time of deposition. Spherical to ovoid-shaped apatite microparticles resembling fossil bacteria are distinct components in the bioclasts. Bone fragments exhibit apatite fillings. The nodules and bone fragments consist entirely of carbonate fluorapatite with low Al, K, and Th concentrations suggesting absence of continental detritus. Shale-normalized REE patterns of the samples support a seawater-derived composition. The highly uniform initial ϵ_{Nd} values of -4.8 to -5.1 are interpreted as the seawater value at the onset of phosphatization ~14 Ma ago. In contrast, $^{87}Sr/^{86}Sr$ ratios show a large range of 0.709055 to 0.709124 corresponding to unusually young stratigraphic ages of ~1 to 3 Ma. The data are interpreted as evidence for post-depositional Sr-exchange of the recrystallizing phosphorites with fluids isotopically not much different from modern seawater. It is concluded that the phosphorites formed under oxic, shallow-water conditions where microbial populations assimilated phosphorus primarily from seawater and mediated precipitation of CFA during early diagenesis at the sediment-water interface on different substrates.

Keywords: Phosphorites; microbial activity; Murray Ridge; REE and trace elements; Sr and Nd isotopes

1. Introduction

Open-ocean phosphorites occur on isolated seamounts, plateaus, ridges, and other elevated areas of the seafloor (Burnett et al., 1987). Not included in this category are those from continental shelves and slopes. Since the discovery of phosphatized limestones at mid-Pacific seamounts by Hamilton (1956), open-ocean phosphorites were reported from the Pacific, Atlantic, and Indian Oceans (Baturin, 1982). The deposits mostly formed under oxidizing conditions, although some can be linked to the equatorial upwelling and mid-water oxygen-minimum zone (Halbach and Manheim, 1984). Phosphatic argillites associated with volcanic material (Kharin, 1974); Guano-derived (Insular-type; Piper, 1986), and marine sedimentary phosphorites (Glenn et al., 1994) are further varieties. Due to the low organic carbon content in open-ocean phosphorites, the sources of phosphorus, e.g. the water column versus submarine volcanism, have been a topic of debate (Glenn et al., 1994). Despite the fact that phosphorite from mid-ocean ridges can account for up to ~12% of the total annual phosphorus input in the oceans (Feely et al., 1996), there are surprisingly few studies on their composition and origin. The purpose of this paper is to elucidate the genesis of phosphorite samples from the Murray Ridge (MR) located near the highly productive upwelling region of the Oman margin (den Dulk et al., 2000). For this purpose we interpret petrological and mineralogical evidence in combination with geochemical- and Nd-Sr isotopic data.

2. Geologic setting, age and description of phosphorite samples

The Murray Ridge (MR) is a ~420 km long and ~20 to 50 km wide NE- trending asymmetric submarine high in the NW Arabian Sea (Fig. 1). It is a shallow oceanic ridge with a water depth of ~400 m at its NE termination (Minshull et al., 1992). It is a part of the Arabian-Indian plate boundary undergoing uplift since the early Miocene (Clift et al., 2002). The ridge is transected by deep discontinuous troughs with a sediment fill of ~2 km. Due to the fact that the sediment layers on the flanks of the MR are of uniform thickness, it can be concluded that the troughs were formed during recent faulting (Uchipi et al., 2002). The summit of the ridge lies within the oxygen minimum zone (OMZ: 150 m - 1250 m; den Dulk et al., 2000) and the formation of the phosphorites may have influenced by upwelling-induced productivity (den Dulk et al., 2000). During the Tertiary and Quaternary the MR was near sea level and probably influenced by transgressive and regressive episodes. The rise and fall of sea level may have

favoured phosphorite accumulation, or aided in reworking and concentrating phosphorite and other authigenic grains (Glenn et al., 1994).

The samples were recovered with a gravity corer from the eastern flank of the MR at 470 m depth (Lat. 21° 24. 4N, Long. 61° 54.7E; Fig. 1). All samples were collected from a single core at 50 cm depth. We studied three different types of phosphorite samples: samples MRP-1 and 2 comprise phosphorite nodules of 1-3 cm diameter (Fig. 2A -2D). Sample MRP-3 is made up of bioclasts (Fig. 2A) consisting of up to 50% of planktonic foraminifers and interspersed basalt and mineral fragments. The planktonic foraminifers (Fig. 2F) are: *Orbulina universa* D'Orbigny' 1839 (base of zone N9 to Recent), *Orbulina bilobata* (D Orbigny, 1846), *Orbulina suturalis* Bronnimann, 1951 (base of zone N9 to Recent), *Praeorbulina sicana* De Stefani, 1950 (base of zone N8 to lower of zone N9), *Globigerinoides trilobus* (Reuss), 1850 (Zone N5 to Recent), *Globigerinoides cf. bisphericus* (lower N7 to lower N9), *Globorotalia archeomenardii* Bolli (Zone N6 to lower N10) and *Globorotalia praemenardii* Cushman and Stainforth (transitional form). According to Postuma (1971) and Bolli and Saunders (1985), a similar age of ~14 -14.5 Ma (Middle Miocene) can be assigned to all of these fossils. Samples MRP-4a and 4b are bone fragments (Fig. 2A, 2E) showing apatite fillings in the bone structure (grey areas in Fig. 2E). The age of the associated sediments is difficult to constrain as the planktonic foraminifers are highly fractured. From the stratigraphic position of the phosphorites from the core there is no convincing evidence to conclude that these phosphorite samples were reworked at the site. There are several findings of Miocene phosphorites in the vicinity of the MR and the NW Arabian Sea (Baturin, 1982; Rao et al., 1992; Rao and Lamboy, 1995; Grandjean et al., 1987) that support widespread phosphatization during the Miocene.

3. Analytical methods

Thin section-, mineralogical- and scanning- electron microscope (SEM) studies were carried out at the National Institute of Oceanography, India. Major- and minor element concentrations were determined by microprobe. The REE- and other trace-element concentrations were determined with ICP-MS, following the method described by Govindaraju (1994). $^{143}\text{Nd}/^{144}\text{Nd}$ ratios were determined on a MAT 261 in a dynamic quadruple mass collection mode. The ϵ_{Nd} values were calculated with the parameters of Jacobsen and Wasserburg (1980). Present-day values for the chondrite uniform reservoir (CHUR) are:

$^{147}\text{Sm}/^{144}\text{Nd} = 0.1967$, $^{143}\text{Nd}/^{144}\text{Nd} = 0.512638$ relative to $^{146}\text{Nd}/^{144}\text{Nd} = 0.7219$. $^{87}\text{Sr}/^{86}\text{Sr}$ ratios were measured in a dynamic double mass collection mode. The NIST 987 reference material yielded $^{87}\text{Sr}/^{86}\text{Sr} = 0.710221 \pm 11$ (N= 22) and the $^{87}\text{Sr}/^{86}\text{Sr}$ ratios in Table 3 are reported relative to 0.710240 in NIST 987. Other details are given in the footnote of Table 3.

4. Results

4.1. Petrological- and mineralogical data

The phosphorite samples are depicted in Fig. 2A. In thin section, the large nodules exhibit homogeneous light-colored micritic phosphate, surrounded by a thin dark-gray phosphate matrix (Fig. 2B). The small nodules reveal phosphate pellets surrounded by a dark-gray phosphate matrix (Fig. 2C). Circular to ovoid and elongated voids are ubiquitous and may represent borings or sites of formerly biogenic detrital particles that dissolved during phosphatization. The relics of microfossils can be found in the center of the pellets (Fig. 2C). The dark-grey portions of the phosphate matrix show a spongy texture with hollow sub-spherical components (Fig. 2D). Elsewhere rounded to ovoid aggregates with obscured internal structure are aligned parallel.

SEM images show bundles of submicron-size micro-filaments wrapping the nucleus of the nodules (Fig. 3A). The filaments are up to 1-2 μm in diameter and comprise several submicron-sized tubules (Fig. 3B). The cortex exhibits a porous nanostructure corresponding to spherical to ovoid cavities ranging from 0.3 to 0.7 μm in diameter (Fig. 3C-D). In some pores, spherical to ovoid-type apatite nanoparticles ~ 0.2 to $0.4 \mu\text{m}$ in diameter form globules that appear to be hollow (Fig. 3E). Filaments commonly extend across the pores. The phosphate in the nucleus of the nodules is dense, yet micro-filaments can be identified (Fig. 3F). Bundled and ramified filaments growing upright and radially into fan-shaped microstructures are shown in Fig. 3G-H.

In the bioclast sample MRP-3 the phosphate is largely confined to the cement (Fig. 2F). It consists of at least two types of apatite particles (Fig. 4A-F): type 1 is gray, spherical, large in size (1-10 μm), and closely packed. This produces a flocculent texture of the matrix (Fig. 4A). Clusters of apatite microparticles of different sizes are set in foraminiferal chambers (Fig. 4B). The calcite of the foraminiferal chambers has been replaced by thread-like apatite (Fig. 4C). In Fig. 4D, hollow, apatite particles of $\sim 2 \mu\text{m}$ are encrusted by nanospheres of apatite. Apatite

particles of type 2 are light brown, smooth-surfaced with smaller ovoids (arrow in Fig. 4E). They occur as aggregates on the surface of type 1 apatite particles (finger in Fig. 4E). There are no internal cavities in the type 2 apatite particles (Fig. 4E). Some apatite particles (Fig. 4F) consist of individual hexagonal crystals piled upon one another, or occur as prismatic crystals. The microstructure of apatite in the cavities of the bone fragments is similar to that of phosphate cement in the bioclats.

The nodule- and bone fragments are composed exclusively of carbonate fluorapatite (CFA). Calcite is also present as a subordinate component in the bioclats. Following the method of Schuffert *et al.* (1990) we estimated a carbonate content of 5 to 6 wt. % in the CFA.

4.2. Geochemical- and $^{87}\text{Sr}/^{86}\text{Sr}$ - and $^{143}\text{Nd}/^{144}\text{Nd}$ isotopic data

4.2.1. Major- and minor element concentrations

The major- and minor element concentrations are listed in Table 1. The average concentrations of CaO (~47 wt. %) and P₂O₅ (~30 wt. %) in the samples are similar to those in phosphorites from other oceans. The CaO/P₂O₅ ratios of 1.52 to 1.55 overlap the value of 1.54 in pure carbonate fluorapatite (McClellan, 1980). CaO/P₂O₅ ratios of 1.51 to 1.54 in authigenic/diagenetic phosphorites from the shelf of Namibia and Peru-Chile are also indistinguishable from the MR data (Table 1). K, Al, and Th concentrations are low and those of the minor elements SiO₂, TiO₂, MnO, K₂O, and Na₂O are similar in the different sample types. The concentration of Fe₂O₃ is highest in the bioclats (~2.4 wt. %) followed by values of ~1.1 to 0.5 wt. % in the nodules.

Among the trace elements, the Sr concentrations of ~2,000 to 2,400 ppm (Table 2) are prominent. Nevertheless, the Sr concentrations are similar to those in biogenic apatite (e.g. Schmitz *et al.*, 1991; Vennemann and Hegner, 1998). The chalcophile elements Cu, Ni, Pb increase in the sequence bone fragments-nodules-bioclats (Table 2) as do the concentrations of the REE and other lithophile elements Cr, Sc, Co, Ga, Y, Zr, Nb, and Th.

4.2.2. The REE data

The Post-Archean Australian Shale (PAAS) -normalized REE abundances in Fig. 5 increase from the LREE to the HREE. The patterns reveal a distinct overabundance of La

relative to Ce, rather than a negative Ce-anomaly. In addition the phosphorite samples show a small and positive Eu-anomaly. For comparison a REE pattern for hydrothermal fluids is shown (Klinkhammer et al., 1994). The prominent positive Eu-anomaly and strong fractionation of light REE over heavy REE in hydrothermal fluids contrast with the pattern of the phosphorite samples and preclude major involvement of hydrothermal fluids in the genesis of the samples.

4.2.3 The $^{87}\text{Sr}/^{86}\text{Sr}$ and $^{143}\text{Nd}/^{144}\text{Nd}$ isotopic ratios

The $^{87}\text{Sr}/^{86}\text{Sr}$ ratios range from 0.709055 in a sample of bone fragments to 0.709124 in the bioclasts (Table 3). Due to the very low Rb/Sr ratio in the samples, their $^{87}\text{Sr}/^{86}\text{Sr}$ isotopic ratios at 14 Ma are indistinguishable from the measured ratios within analytical precision (e.g. the initial ratio is only $\sim 10^{-6}$ lower than the measured ratio). The range in Sr isotopic ratios exceeds the analytical error by a factor of ~ 7 and indicates significant isotopic heterogeneity among the samples. It is noteworthy that the evidence for Sr isotopic heterogeneity also exists in samples of similar composition, e.g. the bone fragments (Table 3). All of these ratios are much higher than the $^{87}\text{Sr}/^{86}\text{Sr}$ isotopic ratio of ~ 0.70885 for seawater at 14 Ma (DePaolo, 1986) and only slightly lower than in modern seawater ratio of 0.709164 (Vennemann et al., 2001). The average stratigraphic ages for the samples as inferred from the seawater curve of Farrel et al. (1995) range from ~ 3 Ma to as young as 0.9 Ma.

The initial ϵ_{Nd} values of -4.8 to -5.1 for an age of 14 Ma are identical within the analytical error of ± 0.3 ϵ -units and contrast the Sr isotopic heterogeneity. They are intermediate between the ϵ_{Nd} value of -3.1 measured in ~ 18 Ma old phosphatic fish debris from the Persian Gulf (Grandjean et al., 1987) and the present-day seawater value for the NW Arabian Sea of -8.3 (Bertram and Elderfield, 1993).

5. Discussion

5.1. Structural evidence for bacterial activity in the nodules

The cortex portions of the nodules show abundant microbial filaments and a spongy texture due to spherical or ovoid-shaped nanocavities (Fig. 3A-D). The cavities resemble microborings caused by endolithic algae/fungi. Perry (1998) reported that microborings caused by cyanophytes, chlorophytes, rhodophytes and fungi dominate in the upper photic zone and

have been used as paleobathymetric indicators of water depth <20 m. Although it is difficult to characterize the organism based on the size of the borings, we suggest that they are caused by endolithic algae/fungi. Dix (1991) reported submicron-size ($\ll 1 \mu\text{m}$) microborings in the intraclasts of limemud sediments. We interpret the presence of microborings (Fig. 3C-D) as evidence for phosphatization in oxic- and shallow-water conditions.

The nucleus of the nodules exhibits micro-laminations and a fan-shaped microstructure (Fig. 3G-H). Golubic (1976) described similar microstructures in stromatolites and explained them with the formation of false branching in heterocystous filamentous cyanophytes. False branching occurs because of intensive cell division at certain zones of the trichome. Within the *Rivulariaceae*, some forms show dichotomously branched bundles of filaments (genus *Gardnerula*) whereas others exhibit cushions of densely branched paint-brush type filaments (*Dichothrix*). We suggest that the fan-shaped microstructure in Fig. 3G-H was produced by *Rivulariaceae* cyanobacteria, which form nodules in particular in intertidal regions (Golubic, 1976). As the microbial filaments themselves were phosphatized, it evidently occurred before the complete decay of organic matter associated with the sheath of the filaments and was probably achieved through metabolic processes during early diagenesis. The microborings and microstructures of the nodules thus lend further support for the hypothesis that phosphatization occurred in oxic, shallow-water.

In Fig. 3E it can be seen that the cortex segment of the nodules shows nanospheres of apatite forming big globules. Calcified nanospheres have been interpreted as former nanobacteria and were reported from many modern and ancient carbonate deposits as well as in laboratory cultures (Folk, 1994; Pedone and Folk, 1996; Chafetz et al., 1998). On the other hand, Kirkland et al. (1999) interpreted nanobacteria-like objects in organic-rich environments as of inorganic origin, yet their precipitation was considered as induced by bacteria. Kajander and Ciftcigglu (1998) and Cisar et al. (2000) doubted the existence of nanobacteria and suggested that biomineralization triggered by biological macromolecules, including phospholipids, can lead to crystallization of apatite nanoparticles.

We have no evidence to decide whether the nanospheres in the nodules are of organic or inorganic origin. Since the apatite nanospheres are located within the cortex of the nodules,

wherein abundant microbial filaments are present, and associated with nanofilaments (Fig. 3E), we presume that microbial activity may have been involved in their formation.

5.2. Structural evidence for bacterial activity in the bioclasts

Type 1 apatite particles are large, flocculate or form clusters of globular bodies in the interstitial pores or in foraminiferal chambers (Fig. 4A-B). They resemble fossilized coccoid cyanobacterial colonies or syngedimentary phosphatized remnants of bacterial cell aggregates, as described by Soudry and Lewy (1990) and Rao and Lamboy (1995). The individual apatite particles or particle clusters are empty (Fig. 4A-B, D) and this finding suggests that the particles are primary and phosphatization was restricted to the external surfaces of the cells. This implies that phosphatization took place during the active metabolic stage of the cells and before the complete decay of organic matter in the cell surface. Martill (1984) suggested that bacterially-induced mineralization is due to spontaneous interaction between biologically-produced metabolites and cations from the environment. It is considered to begin within few hours or days after the death of microbial bodies and proceeds at rapid pace.

The apatite particles of type 2 are smaller than those in type 1, smooth-surfaced and occur as aggregates on the surface of type 1 particles (Fig. 4E). This observation suggests that phosphatization occurred in several steps. These particles are also abundant in ancient and modern phosphorites and were interpreted as fossilized P-rich bacterial cells (O'Brien et al., 1981; Garrison and Kastner, 1990). Van Capellen and Berner (1991) synthesized similar apatite capsules and interpreted them as inorganic components originating from rapid precipitation of phosphate. We find no evidence for an inorganic or organic origin of the particles. However, the laboratory experiments by Hirschler et al. (1990) indicated that bacterial mediation is necessary for phosphorite formation. The crystalline apatites in Fig. 4F may support the arguments of Van Capellen and Berner (1991) who suggested that the initially precipitated phosphate is an amorphous or poorly-crystalline meta-stable calcium phosphate, which transforms into crystalline apatite depending on the degree of supersaturation of fluorapatite. In Fig. 4C it can be seen that dissolution of calcite in the foraminifers and replacement by thread-like apatite seems to be the predominant microbial process. Ehrlich (1996) suggested that bacteria interacting with mineral particles not only lead to dissolution of minerals but may also initiate precipitation of

other minerals. Considering all these findings, we conclude that the microstructures, microbial filaments, and apatite microparticles support an origin of the phosphorites by microbial processes.

5.3. Sources of phosphorus and other elements

Open-ocean phosphorites typically contain high CaO concentrations of 48 to 52 wt.% and CaO/P₂O₅ ratios of 1.7 to 2 (Table 1). The somewhat lower CaO concentrations of 47 to 48 wt.% and CaO / P₂O₅ ratios of 1.52 to 1.54 in the MR phosphorites are similar to those in pure CFA and phosphorites from the organic-rich, high productivity regions off Namibia and Peru (see Table 1). The inferred relatively high carbonate concentrations of 5-6 wt. % and fluoride concentrations of 2.7 to 3.1 wt. % are consistent with a diagenetic environment with very low sedimentation rates (Jarvis *et al.*, 1994). The possible sources of P are discussed below.

(a) *P associated with detritus and oxyhydroxides:* In Table 1 it can be seen that all samples are characterized by low abundances of Al, K, and Th precluding presence of significant amounts of terrigenous matter. Leaching the samples with 6 N HCl produced only ~2.9 wt. % insoluble silicate material in the bioclasts, ~1.2 wt. % in the nodules, and ~0.2 % in the bone fragments (see Fig. 6). Furthermore, we found low Fe₂O₃ concentrations in the samples that are negatively correlated with P₂O₅. These findings imply that P adsorbed on detrital matter or P bound to oxy-hydroxides (Krajewski *et al.*, 1994) cannot represent important sources.

(b) *Fish debris:* Due to the fact that the bone fragments (Fig. 2A, 2F) are associated with the phosphorite samples, it may be speculated if P from fish debris contributed P (e.g., Suess, 1981) to the samples. In view of the overall small amount of fish debris in the sediment, we consider however this source also as not important.

(c) *Organic matter:* Considering that the MR is located close to the highly productive continental margin of Oman, there is the possibility that plankton-derived organic matter may delivered P to the sample site. Considering however, the low concentrations of Ba, Cu, and Zn in the phosphorites we may preclude that such a process must be subordinate. As has been shown by Price and Calvert (1978) and Froelich *et al.* (1988) phosphorites from high-productivity regions (e.g. Namibia and Peru) apparently are characterized by high concentrations of these

elements due to involvement of organic matter from marine plankton. On the other hand, the Cr concentrations in the nodules and bioclasts, and V concentrations in the bioclasts, are high relative to the values in 'average phosphorite' (Table 2). Piper (1991, 1994) reported that Cu, Cd, Cr and V are incorporated in organic matter and may be of a hydrogenous marine or biogenous origin. Brumsack (2006) suggested that Cr is involved in bio-cycling and V usually originates from an early diagenetic source and enters the sediment via diffusion from the water column. The trace element data thus support the notion that the enrichment of elements was due to elemental exchange between the water column and the substrate of the sediment. We suggest that the same process may explain the enrichment of P.

There is abundant evidence of fossil bacteria / cyanobacteria in the bioclasts and nodules (Figs. 3-4) and that phosphatization occurred at oxic, shallow-water conditions. It is therefore plausible that organic matter associated with the microbial filaments, sediment, and seawater supplied the vital elements and that phosphate precipitation was achieved by microbes associated with decaying organic matter at or near the sediment-water interface during early diagenesis.

5.4. The sources of REE, Nd- and Sr-isotopes

The seawater-like REE patterns of the phosphorite samples (Fig. 5) strongly support an origin of the REE (and probably also other elements) ultimately from seawater. The small negative Ce-anomaly in the samples, when compared to that in seawater from the NW Indian Ocean can be explained with the shallow- water conditions at the MR. In such environments Ce is more depleted in surface waters than in deep waters due to its oxidative removal (Bertram and Elderfield, 1993). Small positive Eu-anomalies may be interpreted as evidence for involvement of ridge hydrothermal fluids typically showing a large positive Eu- anomaly due to preferential leaching of REE from feldspars in basalt (Michard et al., 1983; Ruhlin and Owen, 1986; Grandjean *et al.*, 1987; Oudin and Cocherie, 1988; Elderfield, 1988). However, chondrite-normalized REE patterns (not shown) do not show positive Eu anomalies. Thus we need to explain the Eu-anomalies as due to the normalizing procedure using a shale composition. We conclude that the Eu-data preclude involvement of hydrothermal fluids from the basaltic oceanic ridge.

Studies on the behavior of the REEs and Nd isotopes in biogenic apatite (e.g., fish bones, fish teeth, conodonts) have firmly established that the REE are rapidly incorporated from pore waters at the sediment-seawater interface during early diagenesis (e.g., Bernat, 1975; Jarvis, 1984; McArthur and Walsh, 1984; Staudigel et al., 1985; Elderfield and Pagett, 1986; Grandjean et al., 1988; Wright et al., 1987; Oudin and Cocherie, 1988; Stille and Fisher, 1990; Martin and Scher, 2004). Inorganic phases (detrital minerals and oxy-hydroxide flocs) and organic phases (pelletal and organic debris) with REEs scavenged from the water column are considered potential suppliers of REEs to porewaters during early diagenesis (Oudin and Cocherie, 1988). As the acid-insoluble residue of samples MRP 1 to 3 yielded Fe-hydroxide flocs we suggest that the latter contributed a significant portion of seawater-derived REE. This inference is supported by the observation that the bioclast sample MRP 3 with a high Fe-abundance also exhibits high REE concentrations whereas the nodule samples MRP 1 and 2 with lower Fe contents reveal lower REE concentrations. As Nd is known to behave immobile during diagenesis we suggest that the surrounding carbonate-rich sediment typically showing very low Nd concentrations (<1 ppm Nd; Palmer, 1985) has not contributed significant amounts of Nd to the pore fluids and cannot account for the high Nd concentration in some of the samples.

Considering these constraints on the behavior of the REE we interpret the ϵ_{Nd} values of -4.9 and -5.0 in the two samples of bone fragments as the seawater value at ~14 Ma. Due to the fact that the nodule samples as well as bioclast samples yielded within analytical error identical ϵ_{Nd} values as in the two samples comprising bone fragments, it is apparent that they must have formed from the same water mass at ~14 Ma. It is not plausible that the similar ϵ_{Nd} values in the samples could have been produced at different times, as is the case for Sr isotopes (see discussion below), considering that seawater in the modern NW Arabian Sea changed rapidly its composition during the last 18 Ma from a high ϵ_{Nd} value of ~ -3.1 (Grandjean et al., 1987) to a very low value of -8.3 (Bertram and Elderfield, 1993).

Since the Nd isotopic composition in all samples including those with and without evidence for secondary phosphatization is indistinguishable, we suggest that phosphatization occurred in a relatively short time. Alternatively, the most recent phosphatization processes were subordinate and did not affect the primary Nd budget in the samples.

Surprisingly, the $^{87}\text{Sr}/^{86}\text{Sr}$ ratios show a wide range of 0.70906 to 0.70912 and are much higher than ~ 0.70885 for seawater at ~ 14 Ma (DePaolo, 1986). The Sr isotopic range in the samples is slightly lower than the present-day seawater ratio of 0.70916 (Vennemann et al., 2001). The Sr isotopic heterogeneity is also well developed among the two samples comprising bone fragment that yielded ratios of 0.70906 and 0.70910. As the Rb-Sr and Sm-Nd isotopic systems are coupled, resulting in a covariation of $^{87}\text{Sr}/^{86}\text{Sr}$ ratios and ϵ_{Nd} values, it must be concluded that in the light of the uniform ϵ_{Nd} values, the primary Sr isotopic composition of the samples has been altered during diagenesis. The unusually young and diverse ages of 0.9 to 3 Ma as inferred from the Sr isotope curve of Farrel et al. (1995) are consistent with variable degrees of overprinting of the samples with fluids isotopically not much different from modern seawater.

This explanation of seawater overprinting is compelling as involvement of fluids with Sr leached from Indian ridges with low $^{87}\text{Sr}/^{86}\text{Sr}$ isotopic ratios of ~ 0.7025 - 0.7040 would produce a lower value than ~ 0.70885 in the samples as indicated for 14 Ma old seawater. Furthermore, uptake of Sr remobilized from early Miocene and older carbonate rocks and Fe-Mn oxides would also produce $^{87}\text{Sr}/^{86}\text{Sr}$ ratios lower than ~ 0.70885 in the samples. Lastly, involvement of porewaters dominated by radiogenic Sr from old detrital terrigenous minerals with values of ~ 0.71 and higher can be ruled out as the sediment at the MR is carbonate-rich and thus the porewater composition will be controlled by solution-reprecipitation of Sr from carbonate rocks (e.g. Richter and DePaolo, 1987).

It may also be mentioned that evidence for open-system evolution of $^{87}\text{Sr}/^{86}\text{Sr}$ isotopic ratios in phosphorites resulting in reset and unusually young Sr-stratigraphic ages has been reported by e.g., McArthur et al. (1990), Compton *et al.* (1990), Hein et al. (1993), and Stille et al. (1994). Modeling the behavior of Sr during diagenesis of carbonate rocks, Richter and DePaolo (1987, 1988) found that solution-reprecipitation rates decrease significantly with the age and depth of burial of the sediment and that increasing diagenesis resulted in a shift of the $^{87}\text{Sr}/^{86}\text{Sr}$ towards older stratigraphic ages. The latter finding is opposite to that observed in this study. It needs to be mentioned that these results were derived from environments with sedimentation rates of ~ 10 to 40 m/Ma which is 300 to 1,200 times higher than at the MR. In a comprehensive study of porewater, foraminifera, and biogenic apatite (fish teeth) Martin and Scher (2004) reported evidence for Sr isotopic modification towards the composition of

porewater that may be more or less radiogenic than ambient seawater. They interpreted the data with an open-system behavior of Sr involving continuous exchange of Sr in recrystallizing biogenic hydroxy-fluorapatite during burial and diagenesis.

The vulnerability of Sr isotopes in biogenic apatite and by inference phosphorite samples to exchange with porewater, in combination with the extremely low sedimentation rates at the MR provide a framework for interpreting the Sr isotopic data of the MR samples. The observation that the $^{87}\text{Sr}/^{86}\text{Sr}$ ratios in the MR samples are only slightly lower than the present-day seawater ratio suggests that the porewater composition to a depth of at least 50 cm is probably controlled by solution-reprecipitation of recent carbonate material and/or modern seawater. The probably still ongoing Sr exchange in the samples may be facilitated by the porous structure of the samples and in particular the very low burial depth and compaction of the samples.

6. Conclusions

1. Circa 14 Ma old phosphorites from the Murray Ridge are composed of nodules, bioclasts, and bone fragments. The initial substrate of the nodules was an organic-rich microbial mat or pellet, and foraminiferal sediment in the case of the bioclasts. Microborings in the nodules suggest that phosphatization occurred at oxic, shallow-water conditions.

2. During early diagenesis the bacterial populations may have utilized P from pore waters and seawater and they induced precipitation of pure carbonate fluorapatite via metabolic activities at or near the sediment water interface.

3. Trace element- and Sr-Nd isotopic data document seawater as primary source of the chemical composition of the phosphorites. The uniform ϵ_{Nd} values of ~ -5 in the samples are interpreted as representing the seawater value at ~ 14 Ma. The unusually young and highly variable Sr isotopic ages can be explained with resetting of the Sr isotopic record in the samples with ambient seawater-derived Sr.

Acknowledgements

We thank the Directors of the National Institute of Oceanography, Goa and National Geophysical Research Institute, Hyderabad, India for facilities and encouragement. A. Rocholl is thanked for discussions. Part of the analytical work and writing of the manuscript was completed when V. P. R. was a visiting scientist at LMU, Munich, Germany under a Raman Research Fellowship provided by the Council of Scientific and Industrial Research (CSIR), New Delhi. E.H. thanks the German Research Council (DFG) and Indian National Science Academy (INSA) for financial support. We thank Prof. Finn Surlyk, Editor *Palaeo-3* and, Prof. John S. Compton and anonymous reviewers for their critical comments on our manuscript.

References

- Baturin, G.N., 1982. Phosphorites on the sea floor. Origin, composition and distribution. *Developments in Sedimentology* 33, Elsevier Amsterdam.
- Bernat, M., 1975. Les isotopes de l'uranium et de thorium et les terres rares dans l'environnement marin. *Cah. ORSTOM, Series Geology* 7, 65 – 83.
- Bertram, C.J., Elderfield, H., 1993. The geochemical balance of Rare earth elements and Nd isotopes in the oceans, *Geochimica et Cosmochimica Acta* 57, 1957 – 1986.
- Bolli, H.M., Saunders, J.B., 1985. Oligocene to Holocene low latitude planktonic foraminifers. In: Bolli, H.M. (Ed.) *Plankton stratigraphy*, Cambridge University Press, pp. 155 – 262.
- Brumsack, Hans-J., 2006. The trace metal content of recent organic carbon-rich sediments: Implications for Cretaceous Black shale formation. *Palaeogeography Palaeoclimatology Palaeoecology* 232, 344 – 361.
- Burnett, W.C., Cullen, D.J., McMurtry, G.M., 1987. Open-ocean phosphorites – In a class by themselves? In: G. Teleki et al., (Eds.) *Marine Minerals*, D. Reidel Publishing Company, pp. 119 – 134.
- Chafetz, H.S., Akdim, B., Julia, R., Reid, A., 1998. Mn and Fe-rich black travertine shrubs: Bacterially (and nano-bacterially) induced precipitates. *Journal of Sedimentary Research* 68, 404 – 412.
- Cisar, J.O., Xu, D-Q., Thompson, J., Swaim, W., Hu, L., Kopecko, D.J., 2000. An alternative interpretation of nanobacteria-induced biomineralization. *Proceedings of National Academy of Sciences* 97, 11,511 - 11,515.

- Clift, P., Gaedicke, C., Edwards, R., Il Lee, J., Hildebrand, P., Amjad, S., White, R.S., Schlueter, H., 2002. The stratigraphic evolution of the Indus Fan and the history of sedimentation in the Arabian Sea. *Marine Geophysical Research* 23, 223 – 245.
- Compton, J.S., Snyder, S.W., Hodell, D.A., 1990. Phosphogenesis and weathering of shelf sediments from the south-eastern United States: Implications for Miocene $\delta^{13}\text{C}$ excursions and global cooling. *Geology* 18, 1227 – 1230.
- den Dulk, M., Reichart, G.J., van Heyst, S., Zachariasse, W.J., Van der Zwaan, G.J., 2000. Benthic foraminifera as proxies of organic matter flux and bottom water oxygenation? A case history from the northern Arabian Sea. *Palaeogeography Palaeoclimatology Palaeoecology* 161, 337 – 359.
- Depaolo, D.J., 1986. Detailed record of the Neogene Sr isotopic evolution of seawater from DSDP site 590B. *Geology* 16, 103 – 106.
- Dix, G.R. 2001. Origin of Sr-rich magnesium calcite mud in a Holocene pond Basin (Lee Stocking Island, Bahamas). *Journal of Sedimentary Research* 71, 167 – 175.
- Ehrlich, H.L., 1996. How microbes influence mineral growth and dissolution. *Chemical Geology* 132, 5 – 9.
- Elderfield, H., 1988. The ocean chemistry of the rare-earth elements. *Philos. Transaction of Royal Society London A325*, 105 – 126.
- Elderfield, H., Pagett, R., 1986. REE in ichthyoliths: variations with redox conditions and depositional environment. *Science of the Total Environment* 49, 175 – 197.
- Farrel, J.W., Clemens, S.C., Gromet, L.P., 1995. Improved chronostratigraphic reference curve of late Neogene seawater $^{87}\text{Sr}/^{86}\text{Sr}$. *Geology* 23, 403 – 406 .
- Feely, R.A., Baker P.A. Marumo, K., Urabe, T., Ishibashi, J., Gendron, J., Lebon, G.T., Okamura, K., 1996. Hydrothermal plume particles and dissolved phosphate over the superfast-spreading southern East Pacific Rise. *Geochimica et Cosmochimica Acta* 60, 2297 – 2323.
- Folk, R.L., 1994. Interaction between bacteria, nanobacteria and mineral precipitation in hot springs of central Italy. *Geographie physique et Quaternaire* 48, 233 – 246.
- Froelich, P.N., Arthur, M., Burnett, W.C., Deakin, M., Hensley, V., Jahnke, R., Kaul, L., Kim, K., Roe, K., Soutar, A., Vathkanon, C., 1988. Early diagenesis of organic matter in Peru continental margin sediments: phosphorite precipitation In: Burnett, W.C. and Froelich, P.N. (Eds.), *The origin of marine phosphorite: the results of R.V.Robert Conrad cruise 23-06 to the Peru shelf*, *Marine Geology* 80, Elsevier Amsterdam, pp. 309 – 343.

- Garrison, R.E., Kastner, M., 1990. Phosphatic sediments and rocks recovered from the Peru Margin during ODP Leg 112. In: Proceedings of Ocean Drilling Program Scientific Results 112, College station Texas, pp. 111 – 134.
- Glenn C.R., Follmi, K.L., Riggs, S.R., Baturin, G. B., Grimm, K.A., Trappe, J., Abed, A.M., Galli-Olivier, C., Garrison, R.E., Ilyin, A.V., Jehl, C., Rohrllich, V., Sadaqah, R.M.Y., Schidowski, M., Sheldon, R.E., Siegmund, H., 1994. Phosphorus and Phosphorites: Sedimentology and environment of formation. *Eclogae Geolgae. Helvetica* 87, 747 – 788.
- Golubic, S., 1976. Organisms that build stromatolites. In: Walter, M.R. (Ed.), *Stromatolites, Developments in Sedimentology* 20, Elsevier, 113 – 140.
- Govindaraju, K., 1994. Compilation of working values and sample description for 383 Geostandards. *Geostandard Newsletter* 18, (Special issue) 158 pp.
- Grandjean, P., Cappetta, H., Albarède, F., 1988. The REE and ϵ Nd of 40-70 Ma old fish debris from the West-African platform. *Geophysical Research Letters* 15, 389 – 392 .
- Grandjean, P., Cappetta, H., Michard, A., Albarède, F., 1987. The assessment of REE patterns and $^{143}\text{Nd}/^{144}\text{Nd}$ ratios in fish remains. *Earth Planetary Science Letters* 84, 181 – 196.
- Hamilton, E.L., 1956. Sunken Islands of the Mid-Pacific mountains. *Geological Society of America Memoir* 64, Boulder 97 p.
- Halbach, P. , Manheim, F.T., 1984. Potential of cobalt and other metals in ferromanganese crusts on seamounts of the Central Pacific Basin. *Marine Mining* 4, 319 – 336.
- Hein, J.R., Yeh, H-W., Gunn, S.H., Slitter W.V., Benninger, L.M., Wang, C.H., 1993. Two major Cenozoic episodes of phosphogenesis recorded in Equatorial Pacific seamount deposits. *Palaeoceanography* 8, 293 – 311.
- Hirschler, A., Lucas, J., Hubert, J.C., 1990. Bacterial involvement in apatite genesis FEMS. *Microbial Ecology* 73, 211 - 220.
- Jacobsen, S.B., Wasserburg, G.J., 1980. Sm-Nd isotopic evolution of chondrites. *Earth Planetary Science Letters* 50, 139 – 155.
- Jones, E.J.W., Goddard, D.A., 1979. Deep-sea phosphorite of Tertiary age from Annan Seamount, eastern equatorial Atlantic. *Deep-Sea Research* 26A, 1363 – 1379.
- Jarvis, I., 1984. Rare-earth element geochemistry of late Cretaceous chalks and phosphorites from northern France. *Special Publication Geological Survey of India* 17, 179 – 190.
- Jarvis, I., Burnett, W.C., Nathan, Y., Almbaydin. F.S.M., Attia, A.K.M., Castro, L.N., Flicoteaux, R., Hilmy, M.E., Husain, V., Qutawnah, A.A., Serjani, A., Zanin, Y.N., 1994. Phosphorite geochemistry: State-of-the-art and environmental concerns. *Eclogae Geologia Helvetica* 87, 643 – 700.

- Kajander, E.O., Ciftcioglu, N., 1998. Nanobacteria: an alternative mechanism for pathogenic intra- and extracellular calcification and stone formation. *Proceedings of National Academy of Sciences* 95, 8274 – 8279.
- Kharin, G.S., 1974. The phosphatic rocks of the submarine Jan Mayen Ridge (North Atlantic) and their relation to vulcanism. *Litholgiya*. 32 – 35.
- Kirkland, B.L., Lynch, F.L., Rahnis, M.A., Folk, R.L., Milieux, I.J., McLean, R.J.C., 1999, Alternative origins for nannobacteria-like objects in calcite: *Geology* 27, 347 – 350.
- Klinkhammer, G.P., Elderfield, H., Edmond, J.M., Mitra, A., 1994. Geochemical implications of rare earth element patterns in hydrothermal fluids from mid-ocean ridges. *Geochemica et Cosmochemica Acta* 58, 5105 – 5113.
- Krajewski, K.P., Van Cappellen, P., Trichet, J., Kuhn, O., Lucas, J., Martin-Algarra, A., Prevot, L., Tewari, V.C., Gaspar, L., Knight, R.I., Lamboy, M., 1994. Biological processes and apatite formation in sedimentary environments. *Eclogae Geologiae Helveticae* 87, 701 – 745.
- Martill, D.M., 1984. La Fossilisation instantane'e. *La Recherche*, 25, 996 - 1002.
- Martin, F., Scher, H.D., 2004. Preservation of seawater Sr and Nd isotopes in fossil fish teeth: bad news and good news. *Earth Planetary Science Letters* 220, 25 – 39.
- McArthur, J.M., Walsh, J.N., 1984. Rare-earth element geochemistry of the phosphorites. *Chemical Geology* 47, 191 – 220.
- McArthur, J.M., Sahami, A.R., Thirwall, M., Hamilton, P.J., Osborn, A.O., 1990. Dating phosphogenesis with Sr isotopes. *Geochemica et Cosmochim. Acta* 54, 1343 – 1351.
- McClellan, G.H., 1980. Mineralogy of the carbonate fluorapatite. *Journal of Geological Society of London* 137, 675 – 681.
- Michard, A., Albarede F., Michard, G., Minster, J.F., Charlou, J.L., 1983. Rare-earth elements and uranium in high-temperature solutions from East Pacific Rise hydrothermal vent field (13 degree N), *Nature* 303, 795 – 797.
- Minshull, T.A., White, R.S., Barton, P.J., Collier, J.S., 1992. Deformation at plate boundaries around the Gulf of Oman. *Marine Geology* 104, 265 – 277.
- O'Brien, G.W., Harris, J., Milnes, A.R., Veeh, H.H., 1981. Bacterial origin of East Australian continental margin phosphorites. *Nature* 294, 442 – 444.
- Oudin, E., Cocherie, A. 1988. Fish debris record the hydrothermal activity in the Atlantis II deep sediments. *Geochemica et Cosmochemica Acta* 52, 177 – 184.
- Palmer, M.R., 1985. Rare earth elements in foraminifera tests. *Earth Planetary Science Letters* 73, 285 – 298.

- Pedone, V.A., Folk, R.L., 1996. Formation of aragonite cement by nannobacteria in the Great Salt Lake, Utah. *Geology* 24, 763 – 765.
- Perry, C.T., 1998. Grain susceptibility on the effects of microboring, implications for the preservation of skeletal carbonates. *Sedimentology* 45, 39 – 51.
- Piper, D.Z., 1986. Physical and chemical properties of the phosphate deposit on Nauru, western equatorial Pacific Ocean. In: Burnett, W.C and Riggs, S.R. (Eds.), *Phosphate deposits of the world*, v 3, Cambridge University Press, pp. 177 – 194.
- Piper, D.Z., 1991. Geochemistry of a Tertiary sedimentary phosphate deposit: Baja California Sur, Mexico. *Chemical Geology*, 92, 283 – 316.
- Piper, D.Z., 1994. Seawater as a source of minor elements in black shales, phosphorites and other sedimentary rocks. *Chemical Geology* 114, 95 – 114.
- Postuma, J.A., 1971. *Manual of Planktonic foraminifera*. Elsevier Publishing Company, 420 pp.
- Price, N.B., Calvert, S.E., 1978. The geochemistry of phosphorites from the Namibian shelf. *Chemical Geology* 23, 151 – 170.
- Rao, V.P., Lamboy, M., 1995. Phosphorites from the Oman Margin, ODP Leg 117. *Oceanology Acta*, 78, 289 – 307.
- Rao, V.P., Lamboy, M., Natarajan, R., 1992. Possible microbial origin of phosphorites on Error Seamount, Northwestern Arabian Sea. *Marine Geology* 106, 149 – 164.
- Richter, F.M., DePaolo, D.J., 1987. Numerical models for diagenesis and the Neogene Sr isotopic evolution of seawater from DSDP Site 590B. *Earth Planetary Science Letters* 83, 27 – 38.
- Richter, F.M., DePaolo, D.J., 1988. Diagenesis and Sr isotopic evolution of seawater using data from DSDP 590B and 575. *Earth Planetary Science Letters* 90, 382 – 394.
- Ruhlin, D.E., Owen, R.M., 1986. The rare earth element geochemistry of hydrothermal sediments from the East Pacific Rise: examination of a seawater scavenging mechanism. *Geochemica et Cosmochemica Acta* 50, 393 – 400.
- Schmitz, B., Aberg, G., Werdelin, L., Forey, P., Bendix-Almgreen, S.E., 1991. $^{87}\text{Sr}/^{86}\text{Sr}$, Na, Sr, and La in skeletal fish debris as a measure of the paleosalinity of fossil-fish habitats. *Geological Society of America Bulletin* 103, 786 – 794.
- Schuffert, J., Kastner, M., Emanuele, G., Jhanke, R.A., 1990. Carbonate-ion substitution in francolite: a new equation. *Geochemica et Cosmochemica Acta* 54, 2323 – 2328.

- Shaw, H.F., Wasserburg, G.J., 1985. Sm-Nd in marine carbonates and phosphorites. Implications for Nd isotopes in seawater and crustal ages. *Geochemica et Cosmochemica Acta* 49, 503 – 518.
- Soudry, D., Lewy, Z., 1990. Omission-surface incipient phosphate crusts on early diagenetic calcareous concretions and their possible origin, Upper Campanian, southern Israel. *Sedimentary Geology* 66, 151 – 163.
- Staudigel, H., Doyle, P., Zindler, A., 1985. Sr and Nd isotope systematics in fish teeth. *Earth Planetary Science Letters* 76, 45 – 56.
- Stille, P., Fischer, H., 1990. Secular variation in the isotopic composition of Nd in Tethys seawater. *Geochemica Cosmochemica Acta* 54, 3139 – 3145.
- Stille, P., Riggs, S., Clauer, N., Ames, D., Crowson, R., Synder, S.W., 1994. Sr and Nd isotopic analysis of phosphorite sedimentation through one Miocene high-frequency depositional cycle on the North Carolina continental shelf. *Marine Geology* 117, 253 – 273.
- Suess, E., 1981. Phosphate regeneration from sediments of the Peru continental margin by dissolution of fish debris. *Geochemica Cosmochemica Acta* 45, 577 – 588.
- Taylor, S.R., McLennan, S.M., 1985. *Continental crust: its composition and evolution*. Blackwell, Oxford, 311 pp.
- Thomson, J., Calvert, S.E., Mukherjee, S., Burnett, W.C., Bremner, J.M., 1984. Further studies of the nature, composition and ages of contemporary phosphorite from the Namibian shelf. *Earth Planetary Science Letters* 69, 341 – 353.
- Uchupi, E., Swift, S., Ross, D., 2002. Morphology and Late Quaternary sedimentation in the Gulf of Oman Basin. *Marine Geophysical Research* 23, 185 – 208.
- Van Cappellen P., Berner, R.A., 1991. Fluorapatite crystal growth from modified seawater solution. *Geochemica et Cosmochemica Acta* 55, 1219 – 1234.
- Vennemann, T.W., Hegner, E., 1998. Oxygen, strontium, and neodymium isotope compositions of fossil shark teeth as a proxy for the palaeoceanography and palaeoclimatology of the Miocene northern Alpine Paratethys. *Palaeogeography Palaeoclimatology Palaeoecology* 142, 107 – 121.
- Vennemann, T.W., Hegner, E., Cliff, G., Benz, G.W., 2001. Isotopic composition of recent shark teeth as proxy for environmental conditions. *Geochemica et Cosmochemica Acta* 65, 1583 – 1599.
- Wright, J., Shrader, H., Holser, W.T., 1987. Paleoredox variations in ancient oceans recorded by REEs in fossil apatite. *Geochemica et Cosmochemica Acta* 51, 631 – 644.

Figure captions

- Fig. 1. Map of the Arabian Sea and bordering countries. The Murray Ridge and sample locality are indicated.
- Fig. 2. Photographs of phosphorite samples from the Murray Ridge. (A) Different types of phosphorites: N-nodules, Bi-bioclasts, Bo-bone fragments. Thin-section photographs of phosphorite nodules (B-C) at low magnification; (D) matrix of nodules showing spongy texture and minute circular to ovoid cavities, (E) thin-section of a bone fragment showing bone structure and phosphate in voids; (F) thin-section of a bioclast showing planktonic foraminifers and phosphate cement.
- Fig. 3. SEM images of phosphorite nodules. (A-E) cortex segment at different magnifications, showing bundle of microbial filaments (A), microlaminations (B), spherical to ovoid nanocavities (C-D), and apatite nanoparticles forming aggregates in pores (E). Nucleus segment showing a dense matrix with obscured filaments (F) and Rivulariacean cyanobacterial filaments (G-H).
- Fig. 4. SEM images of cement in bioclasts. Apatite microparticles showing flocculent texture (A) and aggregating into clusters in a foraminiferal chamber (B). (C) Foraminiferal chamber wall showing dissolution of calcite and replacement by thread-like apatite structures. (D) Encrustation of apatite nanoparticles on apatite microparticles. (E) Smaller type 1 apatite capsule aggregates (thin arrow) on the surface of larger type 1 apatite particles (finger). (F) Small prismatic and tubular apatite crystals.
- Fig. 5. REE patterns normalized to Post-Archean Australian shale (normalizing data from Taylor and McLennan, 1985). The patterns 1 to 4 refer to the MRP samples in Table 2. For comparison REE patterns for seawater off the Oman margin (Bertram and Elderfield, 1993; concentrations multiplied by 10^6) and hydrothermal vent fluids (Klinkhammer et al., 1994; concentrations multiplied by 10^4) are shown.

Table 1. Major- and minor element concentrations in phosphorite samples from the Murray Ridge (MRP). Concentrations for phosphorites from other localities are listed for comparison.

	MRP 1 Nodules (35)*	MRP 2 Nodules (40)*	MRP 3 Bioclasts (50)*	4 (15)*	5 (20)*	6	7	8 (66)*
SiO ₂	0.05 (b.d.-0.22) ⁺	0.08 (b.d.-0.24)	0.06 (b.d.-0.17)	0.25	1.99	2.78	0.4	4.46
Al ₂ O ₃	0.09 (b.d.-0.76)	0.38 (0.02-1.06)	0.19 (0.02-0.26)	0.19	0.56	n.a.	0.03	1.37
TiO ₂	0.02 (b.d.-0.16)	0.02 (b.d.-0.1)	0.02 (b.d.-0.08)	n.a.	n.a.	n.a.	0.02	n.a.
Fe ₂ O ₃ ⁺⁺	0.49 (0.21-0.51)	1.13 (0.16-7.3)	2.41 (0.10-13.2)	2.53	0.61	n.a.	0.02	1.04
MnO	0.01 (b.d.-0.07)	0.02 (b.d.-0.1)	0.02 (b.d.-0.08)	n.a.	n.a.	n.a.	n.a.	n.a.
MgO	0.94 (0.24-1.2)	0.92 (0.4-1.6)	0.83 (0.55-1.2)	0.49	0.45	0.80	0.71	1.28
CaO	47.5 (45.6-50.0)	47.0 (42.7-51.8)	47.4 (38.4-52.5)	51.97	47.57	50.40	46.21	44.28
Na ₂ O	0.98 (0.22-1.52)	0.95 (0.21-1.53)	0.96 (0.02-0.14)	0.83	0.92	n.a.	n.a.	1.15
K ₂ O	0.06 (0.01-0.22)	0.07 (0.02-0.23)	0.05 (0.4-1.8)	0.13	<0.10	0.13	0.09	0.32
P ₂ O ₅	31.2 (27.6-36.3)	30.4 (26.6-35.5)	30.4 (25.2-34.6)	26.46	27.40	25.30	30.70	28.69
F ⁻	2.73 (1.47-4.63)	2.73 (1.3-4.72)	3.09 (1.33-4.93)	1.20	n.a.	1.99	2.74	3.0
SO ₃ ²⁻	1.5 (1.1-1.8)	2.0 (1.5-4.8)	1.8 (1.2-5.3)	0.97	1.70	n.a.	n.a.	2.10
F/ P ₂ O ₅	0.09	0.09	0.10	0.05	n.a.	0.08	0.09	0.1
CaO / P ₂ O ₅	1.52	1.54	1.55	1.96	1.74	1.99	1.51	1.54

MRP 1, 2, and 3 are samples of this study. * Number of spot analyses by electron microprobe.

⁺ Range of concentrations in all spots. ⁺⁺Total iron as Fe₂O₃.

4 – Phosphorites from the Error Seamount, Owen Ridge, Arabian Sea (Rao et al., 1992).

5 – Phosphorites from Pacific Seamounts (Burnett et al., 1987).

6 – Phosphorites from the Annon Seamount, Atlantic Ocean (Jones and Goddard, 1979).

7 - Authigenic phosphorite pellets from offshore Namibia (sample 5800; Thomson et al., 1984).

8 – Phosphorites from the shelves of Peru and Chile (Burnett et al., 1987).

n.a. = not analyzed.

Table 2. Trace element concentrations in phosphorite samples from the Murray Ridge.

	MRP 1 Nodules	MRP 2 Nodules	MRP 3 Bioclasts	MRP 4a Bone fragments	MRP 4b Bone fragments	Post- Archean shale	MAG 1	Recom- mended* MAG 1
Ba	56.7	56.9	40.5	40.1	39.6	650	485	479
Cu	12.7	15.3	19.7	12.0	12.9	50	30.2	30
Ni	40	43	53	35	36	55	53.6	53
V	75	77	156	69	52	150	142	140
Zn	33	25	30	18	26	85	131	130
Pb	8.1	8.2	12.2	4.8	4.9	20	n.a.	n.a.
Cr	197	83	360	44	39	110	97.5	97
Co	2.9	2.6	7.2	1.2	1.2	23	20.7	20.4
Ga	1.7	1.8	2.0	1.2	1.2	20	20.9	20.4
Rb	3.9	5.2	5.0	1.0	0.7	160	150.9	149
Sr	2360	2380	2010	2060	2150	200	147.3	146
Y	39.8	25.2	56.6	5.2	2.9	27	28.4	28
Zr	16.1	13.6	26.3	2.05	2.48	210	127.6	126
Sc	4.71	3.96	5.23	2.49	2.26	16	17.4	17.2
Nb	1.82	0.98	3.4	0.21	0.26	19	12.17	12.0
Cs	0.26	0.36	0.31	0.04	0.04	15	8.64	8.60
Hf	0.37	0.29	0.50	0.04	0.05	5	3.65	3.70
Ta	0.05	0.04	0.09	0.02	0.01	n.a.	n.a.	n.a.
Th	0.63	0.58	0.86	0.14	0.18	14.6	n.a.	n.a.
U	43.6	61.0	103	72.9	52.7	3.1	n.a.	n.a.
La	10.78	6.70	15.75	1.35	0.96	38	42.86	43
Ce	13.94	8.30	19.48	1.51	1.24	80	88.44	88
Pr	1.93	1.05	2.61	0.23	0.18	8.9	9.38	9.3
Nd	9.24	4.94	12.61	1.02	0.78	32	38.23	38
Sm	2.23	1.14	2.86	0.26	0.24	5.6	7.51	7.5
Eu	0.54	0.29	0.72	0.08	0.07	1.2	1.56	1.55
Gd	2.31	1.22	3.13	0.24	0.19	4.7	5.84	5.8
Tb	0.47	0.25	0.63	0.05	0.04	0.8	0.96	0.96
Dy	3.33	1.85	4.43	0.40	0.25	4.4	5.16	5.2
Ho	0.84	0.49	1.16	0.11	0.07	1.0	1.03	1.02
Er	2.60	1.51	3.48	0.30	0.20	2.9	2.97	3
Tm	0.39	0.25	0.59	0.06	0.03	0.4	0.43	0.43
Yb	2.44	1.55	3.50	0.30	0.17	2.8	2.54	2.6
Lu	0.42	0.27	0.60	0.06	0.03	0.43	0.39	0.40
Eu/ Eu*	0.73	0.75	0.73	0.97	1.0	0.71	0.72	0.72

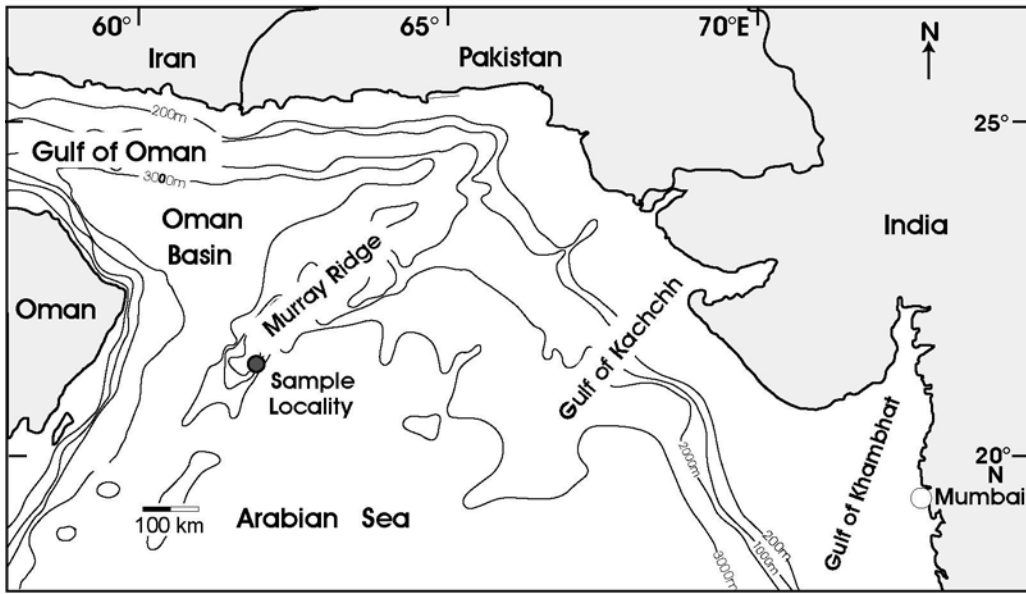
PAAS = Post-Archean Australian Shale (Taylor and McClennan, 1985). MAG-1 Marine mud (International Standard, * Govindaraju (1994), n.a. = not analyzed. $Eu/Eu^* = Eu_n / Gd_n \times Sm_n^{0.5}$, n = normalized to chondrite.

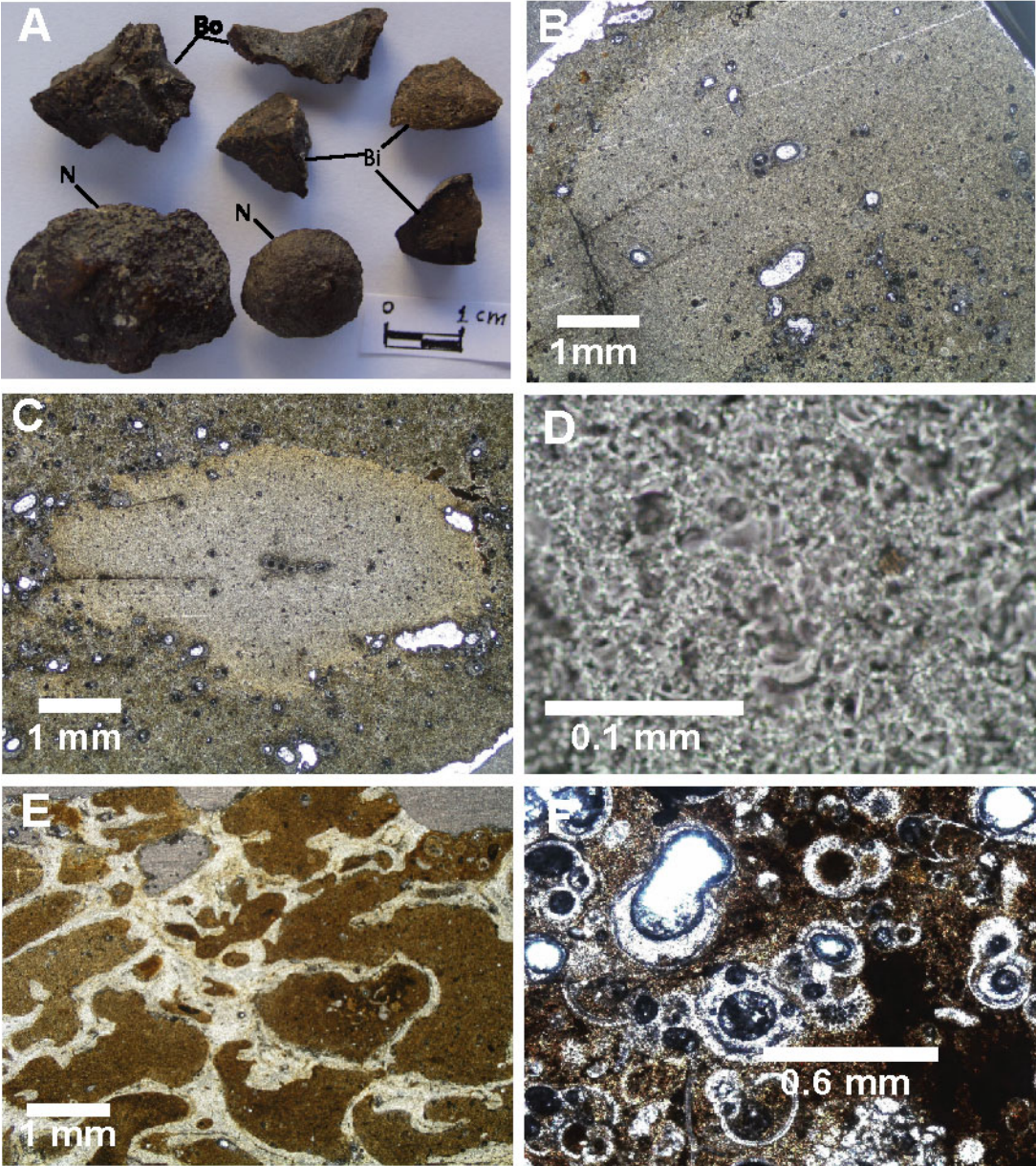
Table 3. Sr- and Nd isotopic data for phosphorite samples from the Murray Ridge

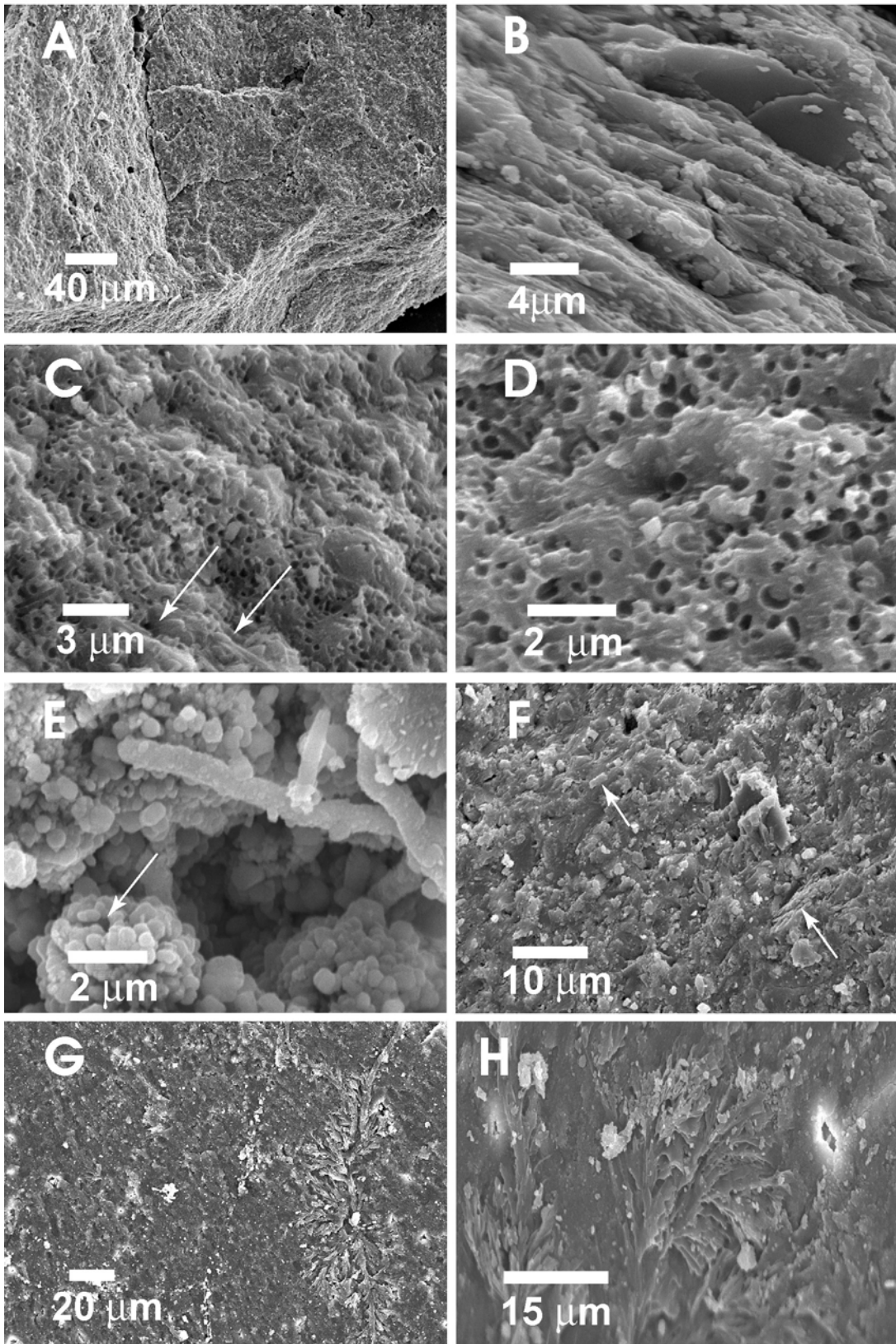
	$^{87}\text{Sr} / ^{86}\text{Sr}(\text{m})$	Strat. age ⁺	Nd	Sm	$^{147}\text{Sm} / ^{144}\text{Nd}$	$^{143}\text{Nd} / ^{144}\text{Nd}(\text{m})$	$\epsilon_{\text{Nd}}(14 \text{ Ma})$
MRP 1 nodules	0.709075 ± 11	~1.9 Ma (1.5-2.7)	9.24	2.23	0.146	0.512370 ± 10	-5.2 (- 5.1)
MRP 2 nodules	0.709098 ± 11	~1.4 Ma (1.1-1.9)	4.94	1.14	0.139	0.512382 ± 14	-5.0 (- 4.9)
MRP 3 bioclasts	0.709124 ± 10	~0.9 Ma (0.6-1.3)	11.85*	2.68*	0.1368	0.512389 ± 10	-4.9 (- 4.8)
MRP 4a bone fragments	0.709055 ± 9	~3 Ma (2-4.3)	1.02	0.78	0.154	0.512385 ± 14	-4.9 (- 4.9)
MRP 4b bone fragments	0.709098 ± 8	~1.4 Ma (1.1-1.9)	0.633*	0.156*	0.1492	0.512377 ± 20	-5.1 (- 5.0)

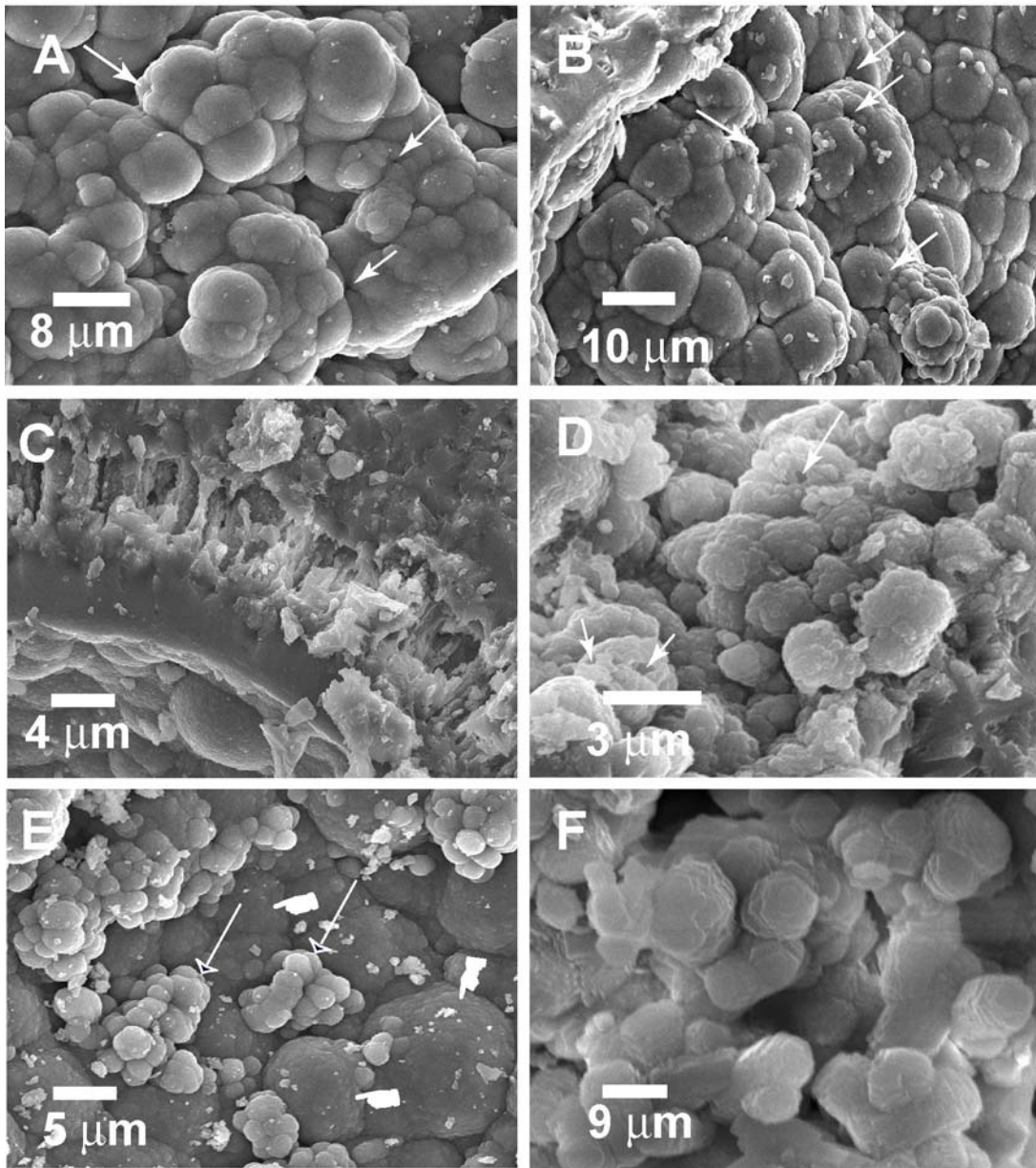
m = measured ratios; ⁺ Stratigraphic age (and age range) inferred from seawater envelope of Farrell et al. 1995. *Determined by isotope dilution, other data by ICP-MS from Table 2. $^{87}\text{Sr}/^{86}\text{Sr}$ normalized to $^{86}\text{Sr}/^{88}\text{Sr} = 0.1194$. External precision for $^{87}\text{Sr}/^{86}\text{Sr}$ is $\sim 1.1 \times 10^{-5}$. $^{87}\text{Sr}/^{86}\text{Sr}$ ratios are relative to 0.71024 in NIST 987. $^{143}\text{Nd}/^{144}\text{Nd}$ normalized to $^{146}\text{Nd}/^{144}\text{Nd} = 0.7219$. External precision for $^{143}\text{Nd}/^{144}\text{Nd}$ is $\sim 1.3 \times 10^{-5}$. The Ames Nd standard solution prepared at Munich yielded $^{143}\text{Nd}/^{144}\text{Nd} = 0.512142 \pm 13$ (2σ , $N = 35$) equivalent to 0.511854 in the La Jolla Nd standard.

Rao et al. Fig. 1









Rao et al. Fig. 5

